Spectral Doppler analysis with sparse and full 2-D arrays

Paolo Mattesini [1,2], Alessandro Ramalli[3,1], Gianluca Goti[1], Lorena Petrusca[2], Olivier Basset[2], Piero Tortoli[1], Hervé Liebgott[2]

[1]*Department of Information Engineering, University of Florence*, Florence, Italy,
[2]*Univ Lyon, INSA-Lyon, UCBL, UJM-Saint Etienne, CNRS, Inserm, CREATIS UMR 5220, U1206 F-69621,* Lyon, France,
[3]*Department of Cardiovascular Sciences, KU Leuven,* 3000 Leuven, Belgium.

***Abstract*—Sparse arrays represent an alternative to full-gridded arrays in 2-D probes realization. Sparse arrays have been used in B-mode imaging tests, but not in spectral Doppler measurements yet. In this paper, we have investigated, by mean of simulations and experiments, how the use of a sparse array instead of a full-gridded 2-D array impacts on spectral Doppler measurements. A 3 MHz, 1024-element gridded array and a sparse array obtained by properly selecting 256 elements from the full array, have been used to interrogate a parabolic flow. Simulations and experiments highlight that the mean Doppler frequency does not change by using the sparse array instead of the full one. Significant differences appear for the bandwidth (17.2% average bandwidth reduction for the sparse array), and for the signal power (22 dB). Possible explanations of this behavior are discussed. Furthermore, it is shown that the empty lines in the 2-D array impact on the Doppler spectra, leading to sidelobes when steering in the direction perpendicular to such lines.**

Keywords—2D arrays, 3D imaging, sparse arrays, spectral Doppler measurements.

I. Introduction

One of the most used modalities for quantitative blood velocity measurements is pulsed wave spectral Doppler imaging [1], which analyzes echoes backscattered from one or multiple [2] sample volumes, contained in the scan plane. The development of 2-D array probes has recently extended Doppler investigation to a volume [3]. However, such probes are usually made of thousands of elements arranged on grids, and individually controlling all of them is quite complex. Possible approaches consist in using application specific integrated circuits (ASICs) [4] or adopting row-column addressing [5]. Otherwise, in sparse arrays [6], a restricted number of elements is spread over the probe surface according to geometries designed to produce the desired acoustic beam. Among many possibilities, these element configurations can be obtained through stochastic optimization processes (like simulated annealing) [7], or by utilizing spiral array geometries [8].

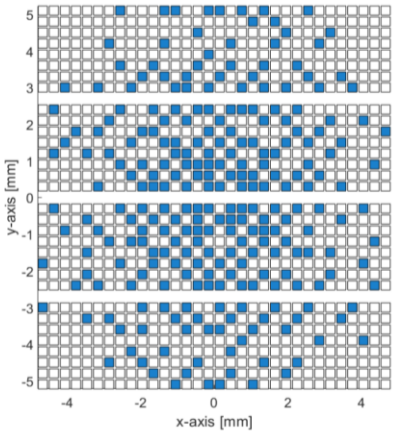

Fig. 1. Active elements distributions used in simulations and experiments. The elements of opti256 (blue) were selected from those available on the ref1024 array (both blue and white elements).

The main goal of this work was to evaluate at what extent the sparsity of probe elements impacts on spectral Doppler measurements.

II. Methods

Simulations and experimental set-up were organized, including a 1024-channels system, a 1024-element 2-D probe and a flow phantom.

A. 2-D array

All tests were based on a 1024-element array probe (Vermon, Tours, France) with a center frequency of 3 MHz. The sparse array configuration was obtained from the full gridded probe configuration by selecting 256 elements according to the simulated annealing algorithm [7]. As explained in [9], the optimization process was exploited by controlling the pressure field behavior at 3 different depths. Fig. 1 shows the layout of the reference full gridded array (ref1024) and the sparse array (opti256).

B. Simulations

In simulations, a continuous flow was established inside a wall-less cylindrical vessel of 5 mm diameter and 24 mm length.

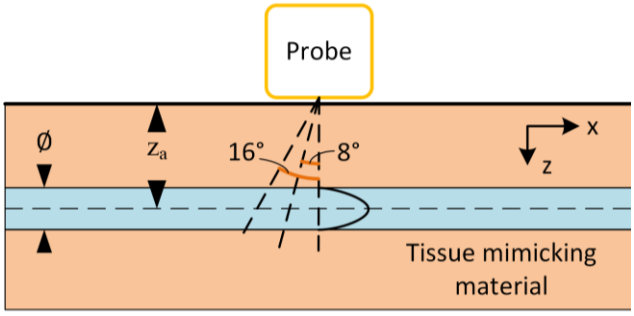

Fig. 2. Schematic of the experimental and simulation set-up.

P. Mattesini was supported by Università Italo-Francese under Grant VINCI 2018.

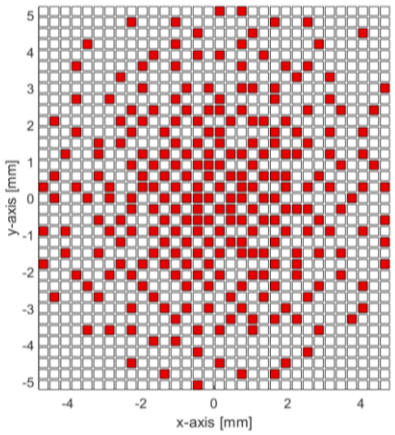

Fig. 3. Active elements distributions used in simulations only. The elements of opti256 v2 (red) were selected from those available on the ref1120 array (both red and white elements).

The point scatterers had a density of 8 scatterers/mm^3 and were moved according to a steady laminar flow with parabolic profile and peak velocity Vp = 40 cm/s. The pipe axis was coincident with the probe x-axis (Fig. 2) at z_a=22.5 mm depth. The pulse repetition frequency (PRF) was 2250 Hz. Field II [10], [11] was used to simulate the acoustic beams associated to the 2-D probe in both ref1024 and opti256 configurations. 5-cycle square bursts at 3 MHz were transmitted, focused on the vessel axis. In reception, dynamic delay-and-sum beamforming without apodization was used. Three steering configurations were tested: 0°, 8° and 16° for both the probe orthogonal planes (xz and yz). For steering within the yz plane, the probe was rotated to maintain the vessel axis parallel to the probe y-axis. Two additional element distributions were simulated (ref1120 and opti256 v2, showed in Fig. 3) to check the effects of the three empty lines in the Vermon probe on the final Doppler spectra.

C. *Experiments*

In the experiments, four Vantage 256 systems (Verasonics, Kirkland, USA) were synchronized to simulate a 1024-channels system [12]. The scanner channels were individually linked to the 1024 elements of the 2D probe and programmed to control the two different sets of element distributions shown in Fig. 1.

The transmission modalities were the same used in simulations. In reception, dynamic focusing without dynamic apodization was used. In each acquisition, raw echo data were stored for a time interval ΔT=0.89 s at PRF = 2250 Hz.

Experiments were based on a Doppler 403 Flow Phantom produced by Gammex (Middleton, WI, USA), which includes a 5-mm diameter vessel surrounded by a tissue mimicking material. A blood mimicking fluid was pumped at 4 ml/s steady rate. Tests were made using the same steering angles used for simulations. In all acquisitions, attention was paid to keep identical set-up conditions for consecutive measurements using ref1024 and opti256 array configurations.

D. *Processing and performance metrics*

Simulated and experimental radio-frequency echo data received from active elements were beamformed off-line, quadrature demodulated, and low-pass filtered using the MATLAB (The MathWorks, Natick, MA) software. The "slow-time" complex samples extracted from each depth (i.e., commonly named Doppler signals), were gathered into overlapping 128-point blocks, each weighted using Blackman-Harris windowing, and then converted to the frequency domain by 128-point FFT. Finally, all the spectra computed for each depth, were averaged.

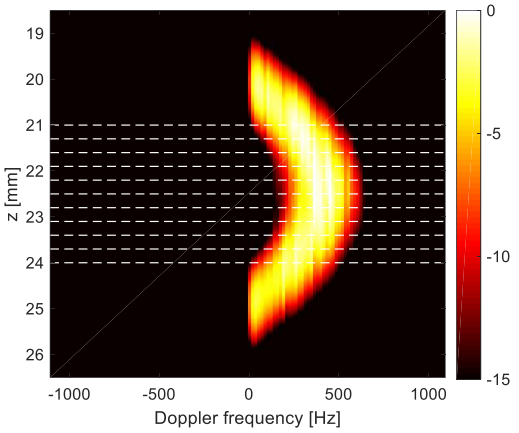

Fig. 4. Example of multi-gate spectral profile obtained in simulation with ref1024 producing a beam steered by 16° on the xz plane.

Fig. 4 shows a sample averaged multi-gate spectral profile obtained in simulation with 16° steering angle on the xz plane. The profile shows the power spectral densities detected between 19 and 26-mm depth. The density of each spectrum is coded according to the color legend on the right.

For every simulated or experimental Doppler spectrum, the mean frequency (Fm), -6dB bandwidth (BW) and signal power (Ps) were evaluated (Fig. 5). Only for experimental data also the signal-to-noise ratio (SNR) was assessed. Ps was evaluated as the integral of the power spectral densities higher than a heuristic threshold (set at -15 dB) reasonably higher than the encountered system noise. As observed in the experimental outcomes, the noise could be assumed as white; hence, its power could be estimated considering the frequency range [–PRF/2 –PRF/4]

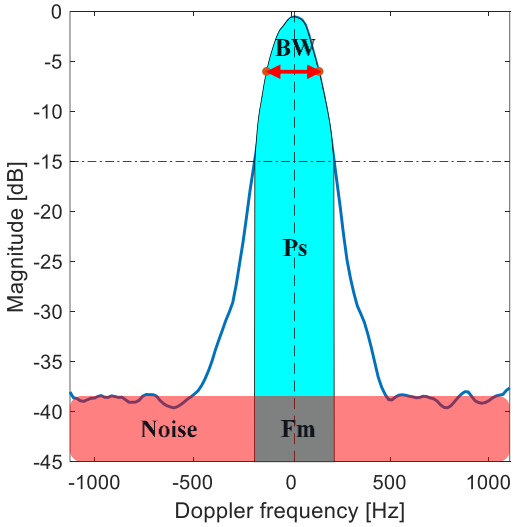

Fig. 5. Sample experimental Doppler spectrum obtained with ref1024 transmitting an unsteered beam. The figure shows how the spectral parameters (fm, BW, Ps and noise) were evaluated.

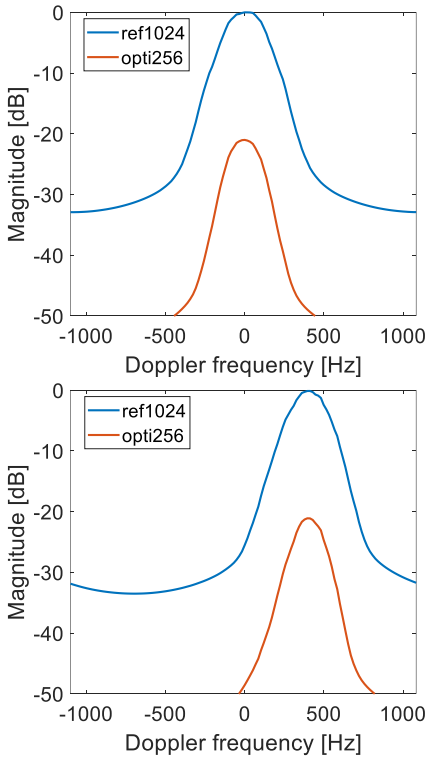

Fig. 6. Examples of simulated Doppler spectra obtained for the two probe configurations at 0° (top) and 16° (bottom) steering angles in xz plane.

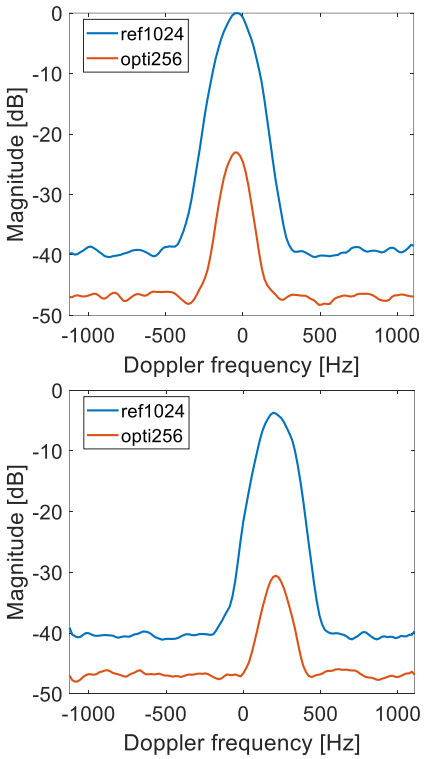

Fig. 7. Examples of experimental Doppler spectra obtained for the two probe configurations when the flow phantom was intercepted by US beams produced with 0° (top) and 16° (bottom) steering angles in xz plane.

that, in all experiments, did not enclose important signal contributions.

In each simulation/experiment, the aforementioned spectral parameters were estimated for the time-averaged spectra obtained at each of 11 depths spaced ≈ 0.3 mm apart (see dotted lines in Fig.4). These depths are in the vessel central zone where flow velocities are clearly higher than zero.

For each depth, the (relative) differences of parameters obtained using ref1024 and opti256 were calculated as:

$$\Delta Fm = \frac{Fm_{opti256} - Fm_{ref1024}}{Fm_{ref1024}} \quad (1)$$

$$\Delta BW = \frac{BW_{opti256} - BW_{ref1024}}{BW_{ref1024}} \quad (2)$$

$$\Delta Ps = \frac{Ps_{opti256}}{Ps_{ref1024}} \quad (3)$$

$$\Delta SNR = \frac{SNR_{opti256}}{SNR_{ref1024}} \quad (4)$$

For each set-up condition, the average value and the associated standard deviation (SD) were evaluated over the 11 depths. The parameters estimated in simulations according to the described procedure are reported in Table I.

III. Results and Discussion

The results in Table I indicate that sparsity does not impact mean Doppler frequency, as confirmed by Figures 6-7-8. On average: for Fm, the difference between ref1024 and opti256 was 0.5%. Conversely, the Doppler bandwidths detected using opti256 are narrower by 17.2%, in average, with respect to the ref1024 ones. This is explained looking at the different equivalent apertures, A, of the two arrays, which involve different Doppler bandwidths [13]. Approximating it as two times the mean distance of each element from the probe center, A resulted 6 and 7.8 mm for opti256 and ref1024, respectively. The ratio between the two apertures (77%) is well consistent with the bandwidth reduction (17.2%, on average) for opti256.

The main difference between the results obtained with 256 or 1024 elements is associated with the signal and the noise power. Using the same TX voltages, we expect 24 dB difference between ref1024 and opti256 signal power. Ps was actually

TABLE I. Simulation Performance Metrics

Steering [°]		opti256 vs ref1024		
xz	yz	$\Delta Fm_{\mu} \pm SD$ [%]	$\Delta BW_{\mu} \pm SD$ [%]	$\Delta Ps_{\mu} \pm SD$ [dB]
0	0	-[a]	-23.5±6.3	-22±0.08
8	0	-0.8±1.7	-19.5±5.4	-22±0.11
16	0	-0.7±1.2	-16±7.9	-21.9±0.04
0	0	-[a]	-15.2±6.5	-22.2±0.48
0	8	1.8±1.9	-15.2±3.1	-22±0.25
0	16	1.5±1.8	-13.5±5.2	-21.9±0.23
Average:		0.5±1.6	-17.2±5.7	-22±0.20

[a] ΔFm not evaluated because the nominal Doppler shift value is here zero

reduced by 22 dB in opti256. On the other hand, the number of channels that contribute to the received noise is 4-times larger for ref1024, i.e., noise is here 6 dB higher. The experimental results (16.8±0.5 dB) look consistent with the expected 24-6=18 dB of SNR degradation. Finally, when the beam was steered on the yz plane, low sidelobes (<-25 dB) appear for ref1024 and opti256 (see Fig. 8). The simulations done with ref1120 and opti256 v2 demonstrate that these sidelobes are associated to the three missing lines on y-direction.

ACKNOWLEDGMENT

The Verasonics systems were co-funded by the FEDER program, Saint-EtienneMetropole (SME) and Conseil General de la Loire (CG42) within the SonoCardioProtection Project supervised by Prof. Pierre Croisille. The authors would to thank LabTAU for their contribution to the 2-D probe experiments, Labex Celya (ANR-10LABX-0060) and Labex PRIMES (ANR-11-LABX-0063) for their support to this research.

REFERENCES

[1] Ph. D. Evans D. H. and W. N. McDicken, Doppler ultrasound: physics, instrumentation, and signal processing, 2nd ed. Chichester ; New York : J. Wiley, 2000.

[2] P. Tortoli, G. Bambi, F. Guidi, and R. Muchada, "Toward a better quantitative measurement of aortic flow," Ultrasound Med. Biol., vol. 28, no. 2, pp. 249–257, Feb. 2002.

[3] J. A. Jensen, S. I. Nikolov, A. C. H. Yu, and D. Garcia, "Ultrasound Vector Flow Imaging—Part I: Sequential Systems," IEEE Trans. Ultrason. Ferroelectr. Freq. Control, vol. 63, no. 11, pp. 1704–1721, Nov. 2016.

[4] E. Kang et al., "A Reconfigurable Ultrasound Transceiver ASIC with 24x40 Elements for 3-D Carotid Artery Imaging," IEEE J. Solid-State Circuits, vol. 53, no. 7, pp. 2065–2075, Jul. 2018.

[5] S. Holbek, T. L. Christiansen, M. B. Stuart, C. Beers, E. V. Thomsen, and J. A. Jensen, "3-D Vector Flow Estimation With Row–Column-Addressed Arrays," IEEE Trans. Ultrason. Ferroelectr. Freq. Control, vol. 63, no. 11, pp. 1799–1814, Nov. 2016.

[6] A. Austeng and S. Holm, "Sparse 2-D arrays for 3-D phased array imaging - design methods," IEEE Trans. Ultrason. Ferroelectr. Freq. Control, vol. 49, no. 8, pp. 1073–1086, Aug. 2002.

[7] E. Roux, A. Ramalli, P. Tortoli, C. Cachard, M. Robini, and H. Liebgott, "2-D Ultrasound Sparse Arrays Multidepth Radiation Optimization Using Simulated Annealing and Spiral-Array Inspired Energy Functions," IEEE Trans. Ultrason. Ferroelectr. Freq. Control, vol. 63, no. 12, pp. 2138–2149, Dec. 2016.

[8] A. Ramalli, E. Boni, A. S. Savoia, and P. Tortoli, "Density-tapered spiral arrays for ultrasound 3-D imaging," IEEE Trans. Ultrason. Ferroelectr. Freq. Control, vol. 62, no. 8, pp. 1580–1588, Aug. 2015.

[9] E. Roux, A. Ramalli, H. Liebgott, C. Cachard, M. C. Robini, and P. Tortoli, "Wideband 2-D Array Design Optimization With Fabrication Constraints for 3-D US Imaging," IEEE Trans. Ultrason. Ferroelectr. Freq. Control, vol. 64, no. 1, pp. 108–125, Jan. 2017.

[10] J. A. Jensen and N. B. Svendsen, "Calculation of pressure fields from arbitrarily shaped, apodized, and excited ultrasound transducers," IEEE Trans. Ultrason. Ferroelectr. Freq. Control, vol. 39, no. 2, pp. 262–267, Mar. 1992.

[11] J. A. Jensen, "FIELD: A Program for Simulating Ultrasound Systems," Med. Biol. Eng. Comput., vol. 34, no. Supplement 1, Part 1, pp. 351–353, 1996.

[12] L. Petrusca et al., "Fast Volumetric Ultrasound B-Mode and Doppler Imaging with a New High-Channels Density Platform for Advanced 4D Cardiac Imaging/Therapy," Appl. Sci., vol. 8, no. 2, Feb. 2018.

[13] P. Tortoli, G. Guidi, and P. Pignoli, "Transverse Doppler spectral analysis for a correct interpretation of flow sonograms," Ultrasound Med. Biol., vol. 19, no. 2, pp. 115–121, Jan. 1993.

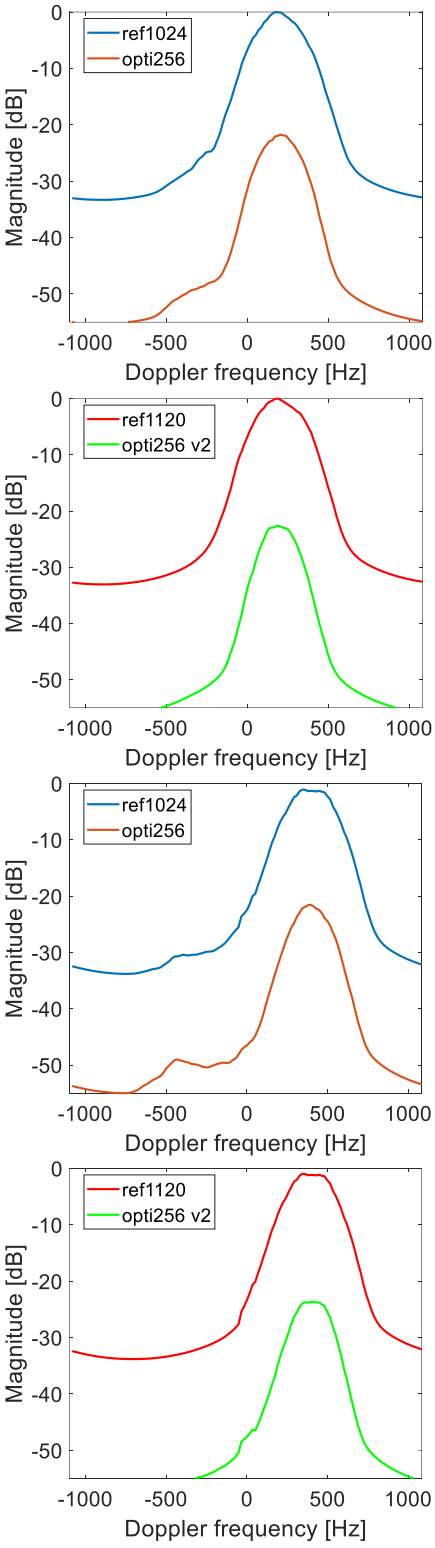

Fig. 8. Doppler spectra comparison between probe configurations with (Fig. 1) and without (Fig. 3) empty lines: obtained at 8° (the two at the top) and 16° (the two at the bottom) steering angles in yz plane.